Feasibility Analysis of Cooling Performance of Passive Containment Cooling System Applicable for OPR1000

Geunyoung Byeon [a], Hyo Jun An [a], Chang Hyun Song [a], JinHo Song [a], Sung Joong Kim [a, b*]
[a]*Department of Nuclear Engineering Hanyang University., 222 Wangsimni-ro, Seongdong-gu Seoul, Korea*
[b]*Institute of Nano Science and Technology, Hanyang University., 222 Wangsimni-ro, Seongdong-gu, Seoul, Korea*
[*]*Corresponding author: sungjkim@hanyang.ac.kr*

Keywords: Passive safety system, MELCOR, PCCS, ECT, LBLOCA

1. Introduction

In the event of a Design Basis Accident (DBA) such as a Loss of Coolant Accident (LOCA) in a nuclear power plant, a significant amount of coolant within the Nuclear Steam Supply System (NSSS) is vaporized into steam, leading to an increase in pressure inside the containment building. This pressure increase jeopardizes the integrity of the containment building, which serves as the final barrier preventing the release of radioactive materials into the environment from the reactor core. Therefore, safety systems to mitigate containment overpressure are essential.

Currently, Korean nuclear power plants, including the Optimized Power Reactor (OPR1000), rely on the Containment Spray System (CSS) to prevent containment overpressure and to remove radioactive materials from the containment atmosphere. However, this system is an active safety system, meaning it may fail to operate in the event of a Station Blackout (SBO) or other power loss accidents, as demonstrated in the Fukushima Daiichi nuclear power plant accident. Thus, the introduction of a passive safety system capable of operating even under power loss conditions is crucial for ensuring the integrity of the containment building.

This study focuses on the design of a passive containment cooling system (PCCS) for the OPR1000 nuclear power plant by using MELCOR 1.8.6 code. In the event of LOCA, where active safety systems are unavailable, the proposed passive containment cooling system aims to maintain containment integrity. The design involves the installation of heat exchangers on the containment building's interior walls and an Emergency Coolant Tank (ECT) outside the containment building. The heat exchangers remove heat from the containment atmosphere, allowing the coolant inside to circulate naturally between the ECT and the containment building.

2. Base Case Scenario Analysis (LBLOCA)

In the design of the OPR1000, a base case analysis was conducted without incorporating mitigation strategies, solely utilizing scenarios where Large-Break Loss of Coolant Accident (LBLOCA) and active safety systems fail to operate. To simulate LBLOCA, a break of 29.5 inches was induced in the cold leg (diameter 30 inches) of the reactor coolant lines, while connecting it to the volume of the containment building's internal atmosphere to simulate coolant leakage. This was simulated by connecting control volumes representing cold leg A1 and the steam generator compartment using flow path 386, as depicted in the nodalization configuration below. The size of the break was simulated by adjusting the size of flow path 386 to represent a 29.5 inches LBLOCA. Furthermore, in the analysis assuming a SBO, the active safety systems were assumed not to operate, while the passive safety systems, such as Passive Autocatalytic Recombiners (PAR) and Safety Injection Systems (SIS), were assumed to be operational.

2.1 Nodalization

The MELCOR nodalization for this LBLOCA base case analysis is as follows:

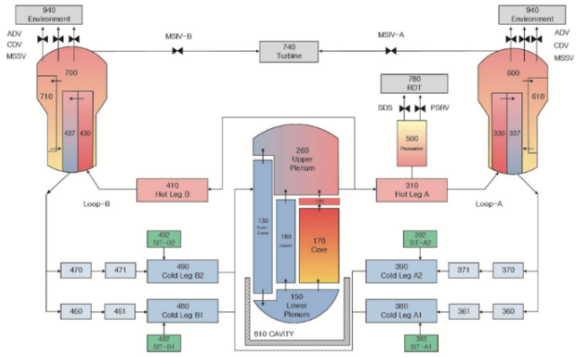

Fig. 1. Nodalization of OPR1000 MELCOR input model [1].

The concrete outer wall of the containment building could also as a heat sink. However, external heat transfer through concrete is considered to be non-dominant compared to heat sink like PCCS. Therefore, it was not modeled in this analysis.

2.2 Analysis Result for Base Case

Table I presents the sequence of events over time for the LBLOCA Base case.

Table I: Event timetable (Base case)

Time (s)	Accident sequence	Remarks
0.022	Accident start (LBLOCA)	
0.314	Stop to supply MFW	
0.326	Reactor trip	

0.339	MSIV (SG) closed	
2.175	Start core uncover	
2.44	Oxidation start	
2.87	RCP trip	SG-A1
10.47	SIT start injection	Loop 1A
24.14	SIT start injection	Loop 2B
306.43	Exhaust SIT	Loop 1A
1000.02	Exhaust SIT	Loop 2B
1888.98	Start to melt cladding	
2190.76	Start to melt or relocation of fuel	
2857.67	Core dry out	
4545.67	UO_2 relocated to lower head	
7040.43	RPV failure	
7390.21	Cavity dryout	
60000.5	Containment leak	Pressure > 0.44MPa [1]
186000.3	Containment failure	Pressure > 1.01MPa [2]

As a result of the LBLOCA at 2.175s, coolant leaked from the Reactor Pressure Vessel (RPV) into the containment building, causing core uncovering and exposing the fuel rods to environment. Subsequently, at 2.44s, oxidation of the fuel zirconium cladding occurred due to steam and oxygen within the reactor.

In this study, a break was induced in the cold leg control volume 380, which is part of the first steam generator loop (Loop 1A) in the OPR 1000 equipped with two steam generators. Therefore, by referencing table I, it can be observed that reactor coolant pump (RCP) at steam generator in loop 1A (SG-A1) tripped at 2.87s. Additionally, the timing of coolant injection from the Safety Injection Tank (SIT) differs between loop 1A and loop 2B. This discrepancy is attributed to the different pressure between the steam generator loops caused by inducing a break in the piping of loop 1A.

Around 2,857s, it can be confirmed that all coolant within the reactor core has evaporated, resulting in core dry out. Subsequently, as there is no coolant present in the RPV for fuel and cladding cooling, temperatures increase, leading to the dissolution of fuel and other materials, eventually causing RPV failure around 7,040s due to heat from the dissolution.

Following RPV failure, molten material is released into the cavity, leading to cavity dry out due to the high temperature of the molten material evaporating all water within the cavity. Subsequent reactions between the molten material and concrete structures generate numerous gases, contributing to an increase in internal containment pressure, ultimately leading to containment leak and containment failure.

Figure 2 illustrates the internal pressure of the containment building obtained through the LBLOCA Base case.

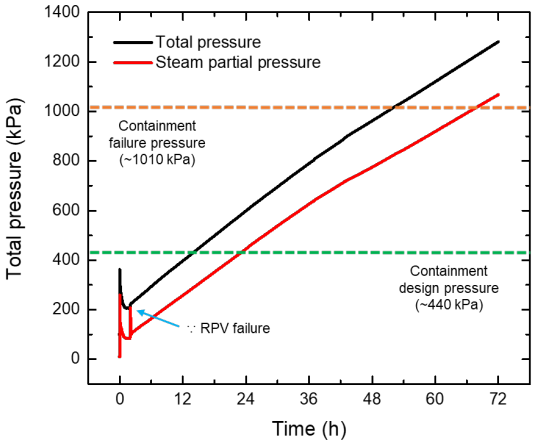

Fig. 2. Pressure changes over time in cavity

When LBLOCA occurs, the coolant within the pipes is discharged in the form of steam into the low-pressure atmosphere. Therefore, it can be observed that the internal pressure of the containment building sharply increases during the initial stages of the accident. Referring to the vapor pressure graph, a sharp increase in pressure can be noted around 7,000s, attributed to the rapid reaction of molten material inside the RPV with water in the cavity following RPV failure. Analyzing the internal pressure of the containment building in the base case indicates that containment failure may occur around two days after the accident if mitigation measures are not implemented.

2.3 ECT Capacity Calculation from Base Case Result

Prior to designing the PCCS, the capacity of the ECT was determined based on the results of the base case. In selecting the ECT capacity, the major heat sources during accidents, namely decay heat (Figure 3) is considered.

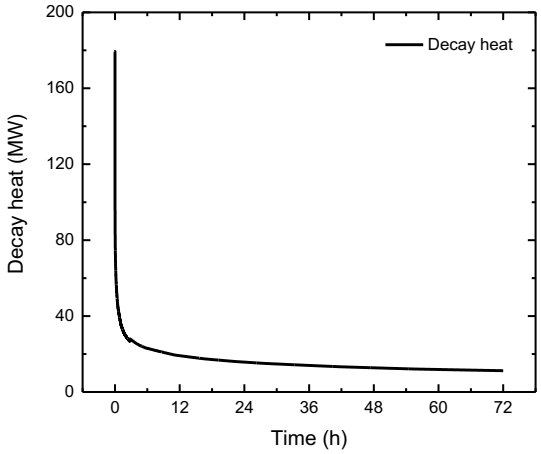

Fig. 3. Predicted decay heat in OPR1000

Utilizing this information, the total energy was calculated via a Riemann sum, and the volume of the ECT was determined based on the energy required for 1 atmosphere of water to vaporize at 35 °C. The energy

from oxidation heat was not considered in this analysis as it accounts for approximately 1% of the energy from decay heat. The temperature of water was set to 35 °C considering the operation of the system even during normal reactor operation, accounting for the internal temperature of the containment building (approximately 48 °C). The final volume of the ECT was calculated assuming it would remove decay heat for 72h, with 40% of coolant present in the ECT. This calculation is summarized in Table II below.

Table II: ECT Capacity Calculation

Total decay heat over 72h (a)	4.11×10^6 MJ
Total oxidation heat over 72h	4.75×10^4 MJ
Water heat removal capacity (b)	2,528.78 kJ/kg
Required ECT coolant volume	1,624.24 m^3
Total amount of ECT coolant	2,240.0m^3

Using the calculated ECT volume, the width, length, and height of the ECT for the reference case analysis were set to 16m, 14m, and 10m, respectively.

3. Reference Case Analysis

3.1 Assumptions & Design Conditions

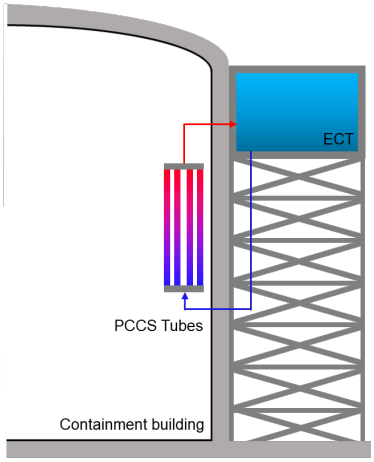

Fig. 4. PCCS design concept (for OPR1000)

For the design of the passive containment cooling system, as depicted in Figure 4, an approach was devised wherein a heat exchanger is installed on the inner wall of the containment building, and an ECT is positioned outside the containment structure. In this configuration, the coolant within the heat exchanger tubes remove heat from the containment building's atmosphere, subsequently becoming heated and naturally circulating between the emergency coolant tanks.

Regarding the design assumptions, an LBLOCA scenario was selected without the injection of mitigation measures. However, only the injection of active safety systems was limited, while passive safety systems such as PAR were assumed to be operational. Additionally, it was presumed that heat transfer from the containment building's interior to the PCCS heat exchanger occurs even during normal reactor operation, without additional valves between the ECT and PCCS. The process of condensed water from the PCCS heat exchanger moving to the In-containment Refueling Water Storage Tank (IRWST) for recirculation was not included in this analysis. Lastly, as the heat transfer area increases, the condensation efficiency improves, which significantly impacts the pressure reduction within the containment building. Therefore, in this study, the heat transfer area was kept constant, while the effects of other variables were evaluated.

For the design conditions, the angle of the PCCS heat exchanger was set as a tube bundle perpendicular to the ground. This decision was based on previous studies indicating that the impact of the angle on temperature and pressure is negligible compared to other factors [3].

Despite being set as a tube bundle, the analysis was conducted using single tubes based on previous literature indicating no significant difference in the results of heat transfer simulations between single tubes and tube bundles in the actual MELCOR analysis [4]. Therefore, the volume for one tube was input as the total volume of the bundle, and hydraulic diameters, etc., were input based on values for one tube to simulate multiple tubes.

3.2 Used Models (MELCOR)

In this analysis, considering condensation heat transfer as a predominant heat transfer mechanism, an investigation was conducted on the condensation heat transfer models within MELCOR prior to the analysis. The relevant models in this analysis include the mass transfer coefficient in phase change heat transfer, natural convection heat transfer coefficient due to natural circulation calculations within the ECT, diffusion model when non-condensable gases (NCGs) are mixed with steam, and the film heat transfer coefficient for condensate. As the interior of the reactor is relatively large in scale, filmwise condensation is considered the primary condensation heat transfer mechanism compared to dropwise condensation [5]. The counter-current model is included in the latest version of MELCOR, but it is not included in the MELCOR 1.8.6 version used in this analysis [6]. A summary of the correlations used in this MELCOR analysis is presented in Table III below.

Table III: Correlation used in MELCOR analysis [7]

Mass transfer coefficient (Heat & Mass transfer analogy)
(1) $Sh = NuSc^{1/3}Pr^{-1/3}$ (2) $j_{cond} = Sh\frac{D}{L}$
Natural convection heat transfer (Chulchill-Chu correlation)
(3) $Nu_{laminar} = 0.59(GrPr)^{1/4} \quad Ra < 10^9$ (4) $Nu_{turbulent} = 0.10(GrPr)^{1/3} \quad Ra > 10^{10}$

Diffusion model (Rohsenow correlation)
(5) $Nu = 0.13(GrPr)^{1/3}$ (6) $Sh = 0.13(GrSc)^{1/3}$
Condensate film HTC (Kutateladze correlation)
(7) $Re_f = \frac{4\Gamma}{\mu_f}$

3.3 Heat Transfer Area Calculation

The heat transfer area of the PCCS heat exchanger was determined based on previous research, utilizing the ratio of reactor output to OPR1000 thermal output, resulting in a heat transfer area of 817.72 m². Using the assumed heat transfer area from previous research [8], the shape information of the PCCS tubes was arbitrarily set based on ASME specifications. This is summarized in Table IV.

Table IV: Calculated dimension of PCCS (for OPR1000)

Parameter		Value
PCCS Tube	Inner / Outer diameter [m]	0.0448 / 0.0508
	Length [m]	5
	Number of tubes [ea]	252
ECT	Width [m]	16
	Length [m]	14
	Height [m]	10

3.4 Nodalization

Based on the geometry information provided above, nodalization was constructed for MELCOR analysis, as shown in Figures 5. In this reference case analysis, the location of the ECT is positioned outside the containment building, with its height situated around 35m from the ground level.

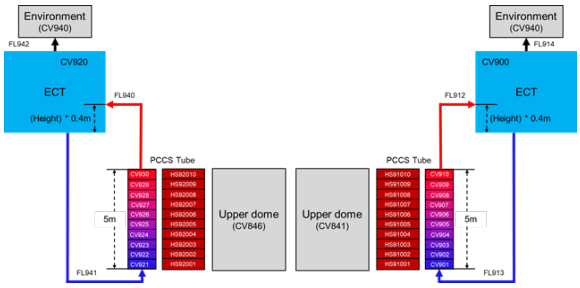

Fig. 5. Nodalization for reference case analysis

3.5 Result

Referring to Figure 6, it can be observed that the installation of PCCS leads to a reduction in internal pressure within the containment building to approximately one-third compared to the base case. Furthermore, it is noted that even after 72h following the accident, the internal pressure of the containment building remains near the design pressure and leak criteria of 0.44 MPa.

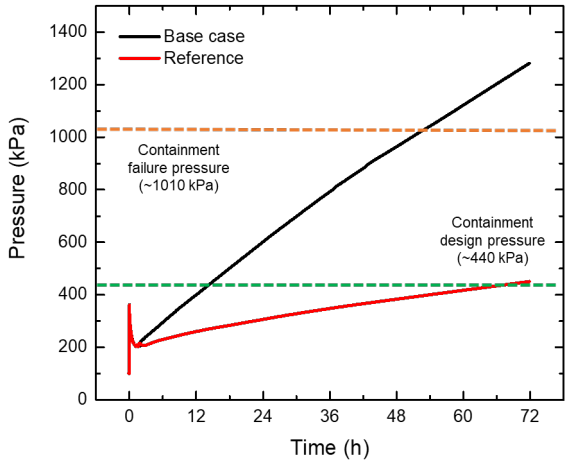

Fig. 6. Changes in pressure within the containment

Figure 7 illustrates the flow velocities resulting from natural circulation of coolant in the ECT and PCCS. The flow velocities are approximately 0.07 m/s for all tubes in the PCCS and 0.03 m/s for the ECT. A peak velocity is observed at the beginning of the accident, attributed to the rapid temperature increase caused by the large amount of steam released initially.

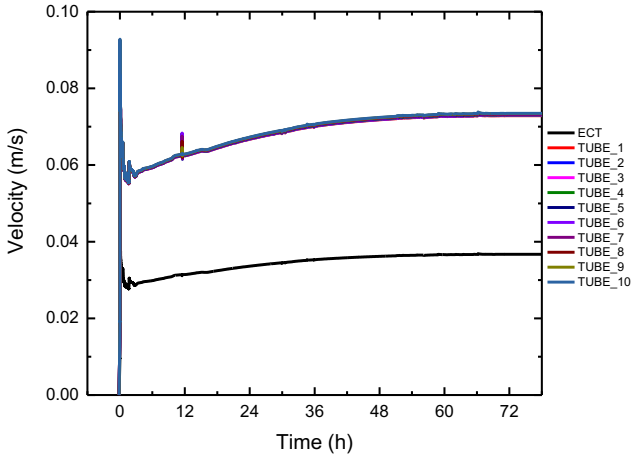

Fig. 7. Changes in natural circulation velocity

Figure 8 depicts the temperature variations over time in the ECT and PCCS. Tube 1 represents the PCCS control volume near the ground, while Tube 10 represents the control volume further away from the ground. As similar magnitudes of natural circulation occur, temperature differences between tubes are observed at similar intervals. Contrary to the assumption of boiling occurring within the ECT, no boiling was observed based on the temperature graph in Figure 8 and the water level graph in Figure 9.

Figure 10 and Figure 11 illustrate the graphs of temperature changes over time at the interface between the coolant and PCCS tubes heat structure and the pressure changes over time within the control volumes of ECT and PCCS, respectively. The temperature in the heat structure reaches a maximum of about 120°C, while the minimum pressure in the PCCS control volume, as

shown in Figure 11, is approximately 300 kPa, indicating that subcooled boiling does not occur at this saturation temperature of 133.5°C [9].

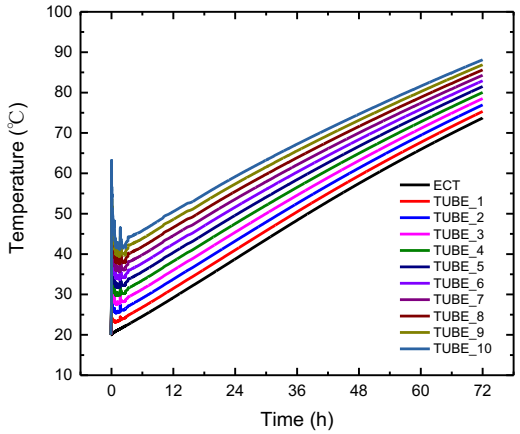

Fig. 8. Changes in liquid temperature within the control volume

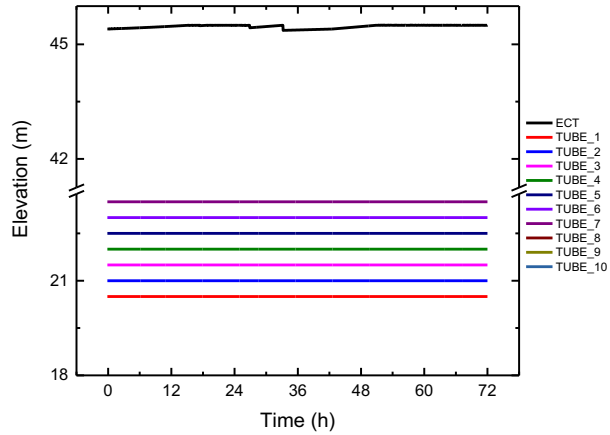

Fig. 9. Changes in liquid elevation within the control volume

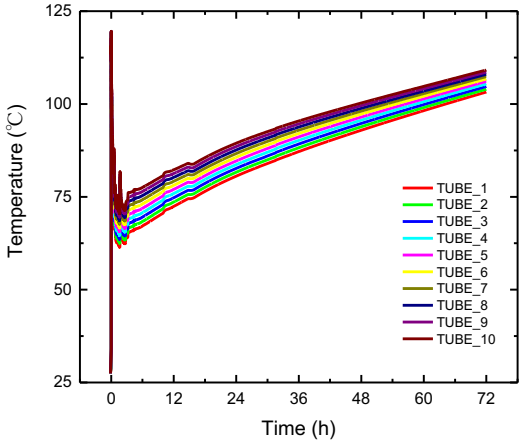

Fig. 10. Temperature changes in each heat structure

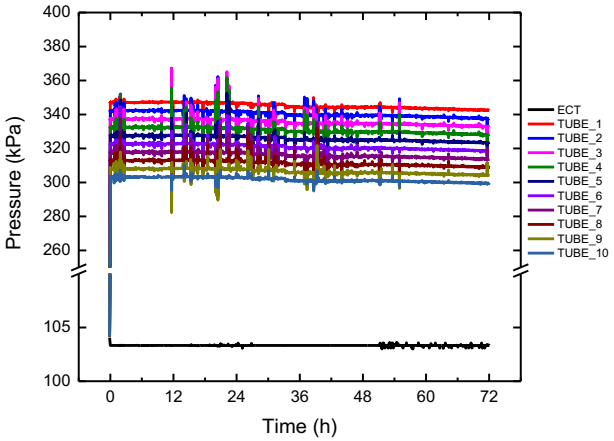

Fig. 11. Pressure changes in each control volume over time

Based on the reference case analysis results, it is noted that natural circulation occurs, and boiling does not occur. Therefore, in the subsequent parametric analysis section, comparisons were made only for the maximum pressure within the containment building during the 72h following the accident.

4. Parametric Analysis

In this analysis, an examination was conducted on the peak pressure within the containment building for 72h following the accident by varying only the shapes of the ECT and PCCS tubes while maintaining the same heat transfer area for the PCCS. Since changes in heat transfer area have a significant impact on pressure reduction within the containment building, no analysis was performed on variations in heat transfer area.

4.1 Test Matrix

The evaluation of the ECT shape considered factors such as the installation location of the ECT, differences in ECT dimension with the same coolant capacity, and variations in the number of ECTs with the same total coolant capacity.

For the PCCS tube shape, an assessment was made based on differences in diameter and length, while adjusting the number of PCCS tubes to maintain the same heat transfer area. This information is summarized in Table V. In Table V, Case I serves as the reference case. Additionally, Case IV, VII, and X are identical to Case I (reference case).

Table V: Test matrix

Component	Parameter	Value [m]	Remark
ECT	Position (Elevation)	35	Case I
		53	Case II
	Dimension	16 × 28 × 2.5	Case III
		16 × 14 × 5.0	Case IV
		16 × 7 × 10.0	Case V
PCCS Tube	Diameter	0.0254 / 0.0194	Case VI

	(O.D. / I.D.)	0.0508 / 0.0448	Case VII
		0.0762 / 0.0702	Case VIII
	Height	2.5	Case IX
		5.0	Case X
		7.5	Case XI

4.2 Result & Discussion

Table VI ~ IX summarizes the maximum pressure inside the containment building within 72h after the accident for each case. Since the analysis did not consider variations in heat transfer area as a variable, it was observed that the maximum pressure inside the containment building differs minimally, at the level of 2%, between the Reference case (Case I) and each respective case.

4.2.1 Position of ECT (Case I ~ Case II)

In Figure 12, it can be observed that there is no difference in the partial pressure of steam within the containment building's control volume in the base case. However, referring to Case I and II in Table VI, it was noted that the cooling performance within the containment building is effective when the ECT is positioned at the highest point. This was attributed to the differences in volume among the components of the containment building's control volume as inputted in MELCOR. While the analysis showed that the cooling performance is effective when both the ECT and PCCS tubes are located at the highest point of the containment building, the ECT height of 53m applied in the input was deemed unrealistic as the PCCS tube is realistically located inside the hemispherical dome of the containment building. Therefore, in subsequent analyses, the ECT position was set to 35m above ground level.

Table VI: Maximum pressure within the containment building according to position of ECT

Case number	Containment maximum pressure [kPa]
Base case	1281.43
Case I	456.81
Case II	451.04

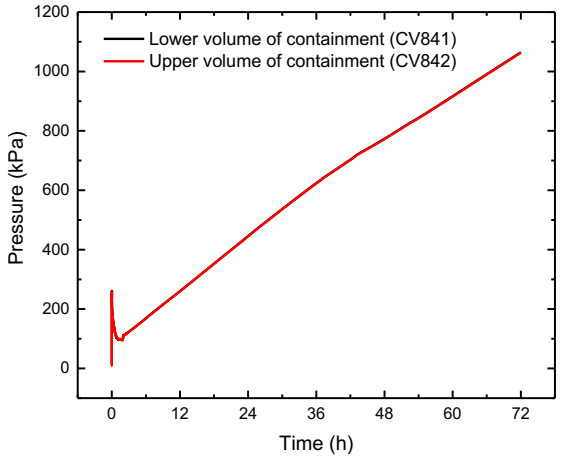

Fig. 12. Steam partial pressure (Base case)

4.2.2 Dimension of ECT (Case III ~ Case V)

In Table VII, it can be observed that the cooling performance within the containment building is most efficient when the height of the ECT is highest, attributed to the increased head due to the longer height of the ECT.

Table VII: Maximum pressure within the containment building according to dimension of ECT

Case number	Containment maximum pressure [kPa]
Case III	451.47
Case IV	456.81
Case V	451.23

4.2.3 Diameter of PCCS (Case VI ~ Case VIII)

In Table VIII, it was found that using a medium-sized diameter (Case VII, 2 inches) for the PCCS tube results in effective cooling performance within the containment building. Since the design of this system is based on natural circulation, it was assumed that a smaller diameter of the pipe and a greater temperature difference between the inlet and outlet of the cooling water in the PCCS tube would lead to more efficient cooling. However, referring to the flow rate data of the PCCS in Figure 13 for different cases, it can be noted that the natural circulation flow rate for Case V with a medium-sized diameter tube is greater than that of Case VI with the narrowest tube. Therefore, it was concluded that this discrepancy is attributed to pressure drop caused by friction within the coolant and the tube.

Table VIII: Maximum pressure within the containment building according to diameter of PCCS

Case number	Containment maximum pressure [kPa]
Case VI	460.71
Case VII	456.81
Case VIII	456.93

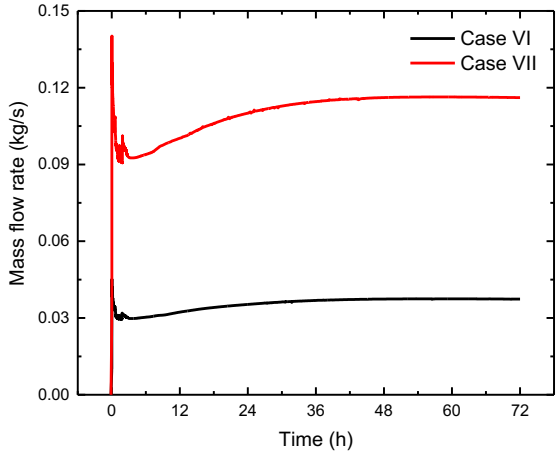

Fig. 13. Mass flow rate in PCCS tube (Case VI, Case VII)

4.2.4 Height of PCCS (Case IX ~ Case XI)

In Table IX, it was found that, from the perspective of cooling performance within the containment building, Case XI with the longest tube length (7.5m) among three scenarios shows marginal effectiveness in terms of cooling.

Table IX: Maximum pressure within the containment building according to height of PCCS tubes

Case number	Containment maximum pressure [kPa]
Case IX	457.24
Case X	456.81
Case XI	456.71

5. Summary

The purpose of this study is to assess the integrity of the containment building by adding the PCCS to the OPR1000 when the Active Safety System is not functioning. To achieve this goal, a test matrix was selected for the configuration of both ECT and PCCS components, and the heat transfer area of PCCS was uniformly set across all cases. Variables for ECT included evaluating installation height and height, while parameters for PCCS tubes involved assessing height and diameter. As the heat transfer area was kept consistent across all calculations, the maximum pressure within the containment building during the 72h post-accident did not vary significantly for each case. However, differences in the shapes of ECT and PCCS ultimately affected their performance in heat transfer due to their influence on natural circulation behavior.

6. Acknowledgement

This work was supported by the National Research Foundation of Korea (NRF) grant funded by the Korean government (MSIT: Ministry of Science and ICT) (No. RS-2022-00144202).

Additionally, this work was supported by the Innovative Small Modular Reactor Development Agency grant funded by the Korea Government (MSIT) (No. RS-2023-00259516).

REFERENCES

[1] Choi, Wonjun, et al. "Effect of molten corium behavior uncertainty on the severe accident progress." Science and Technology of Nuclear Installations 2018 (2018).

[2] Lee, Sang-Won, et al. "Containment depressurization capabilities of filtered venting system in 1000 MWe PWR with large dry containment." Science and Technology of Nuclear Installations 2014 (2014).

[3] Du, Wang-Fang, et al. "Numerical simulation and parameter sensitivity analysis of coupled heat transfer by PCCS containment wall." Applied Thermal Engineering 113 (2017): 867-877.

[4] Bang, Jungjin, et al. "Parametric analyses for the design of a closed-loop passive containment cooling system." Nuclear Engineering and Technology 53.4 (2021): 1134-1145.

[5] Bhowmik, Palash K., Joshua P. Schlegel, and Shripad Revankar. "State-of-the-art and review of condensation heat transfer for small modular reactor passive safety: Experimental studies." International Journal of Heat and Mass Transfer 192 (2022): 122936.

[6] Humphries, Larry LaRon. MELCOR Overview. United States: N. p., 2012. Web.

[7] Gauntt, R. O., et al. "MELCOR computer code manuals." Sandia National Laboratories, NUREG/CR 6119 (2000): 785.

[8] Lee, Sang Won, et al. "The concept of the innovative power reactor." Nuclear Engineering and Technology 49.7 (2017): 1431-1441.

[9] Robert L. Brown and Stephen E. Stein, "Boiling Point Data" in NIST Chemistry WebBook, NIST Standard Reference Database Number 69, Eds. P.J. Linstrom and W.G. Mallard, National Institute of Standards and Technology, Gaithersburg MD, 20899, https://doi.org/10.18434/T4D303, (retrieved March 11, 2024).